ResearchGate

See discussions, stats, and author profiles for this publication at: https://www.researchgate.net/publication/243374800

Phase Stability, Structural Transition, and Hydrogen Absorption−Desorption Features of the Polymorphic La 4 MgNi 19 Compound

ARTICLE *in* THE JOURNAL OF PHYSICAL CHEMISTRY C · JULY 2010

Impact Factor: 4.77 · DOI: 10.1021/jp103910e

CITATIONS
32

READS
20

7 AUTHORS, INCLUDING:

Liuzhang Ouyang
South China University of Technology
152 PUBLICATIONS **1,520** CITATIONS

SEE PROFILE

M. Zhu
South China University of Technology
235 PUBLICATIONS **2,722** CITATIONS

SEE PROFILE

Available from: Liuzhang Ouyang
Retrieved on: 31 January 2016

Phase Stability, Structural Transition, and Hydrogen Absorption−Desorption Features of the Polymorphic La_4MgNi_{19} Compound

Qingan Zhang,*,† Miaohui Fang,† Tingzhi Si,† Fang Fang,‡ Dalin Sun,‡ Liuzhang Ouyang,§ and Min Zhu*,§

School of Materials Science and Engineering, Anhui University of Technology, Maanshan 243002, China, Department of Materials Science, Fudan University, Shanghai 200433, China, and School of Materials Science and Engineering, South China University of Technology, Guangzhou 510641, China

Received: April 29, 2010; Revised Manuscript Received: May 27, 2010

The phase stability, structural transition, and hydrogen storage characteristics of the polymorphic La_4MgNi_{19} compound are systematically investigated in the present work. The La_4MgNi_{19} compound has two variants in the temperature range of 840−960 °C with a preference for a hexagonal structure (2H) at a higher temperature and a rhombohedral structure (3R) at a lower temperature. Because the structure and composition are almost identical, the polymorphic transition between the 2H and 3R phases may proceed through short-range displacements of their subunit layers. Detailed analyses on XRD patterns for the hydrided or dehydrided samples indicate that the equilibrium pressures of hydrogen absorption and desorption for the 2H phase are lower than the pressures for the 3R phase, but the pressure gap between the two phases is too small to be identified from the measured pressure−composition (*P*−*C*) isotherms. The average hydriding and dehydriding enthalpies are determined to be −32.1 and 31.5 kJ/mol H_2, respectively. As hydrogen atoms enter into the lattices, the strains in both the 2H and the 3R phases increase first in the region of the dilute H-dissolved solid solutions and then dramatically decrease once the dilute solid solutions transform into the corresponding hydrides.

Introduction

As hydrogen storage materials, ternary R−Mg−Ni (R = rare earth metals or Ca) compounds have been studied because their hydrogen storage properties are superior to those of corresponding R−Ni compounds.[1–15] These R−Mg−Ni compounds have layered structures with the general formula of $m[RMgNi_4]\cdot n[RNi_5]$ or $R_{n+m}Mg_mNi_{5n+4m}$,[15–18] in which $[RMgNi_4]$ (Laves-type) and $[RNi_5]$ (AB_5-type) subunits stack along the *c* axis alternatively according to certain combinations.[16,17] The numbers, *m* and *n*, for $[RMgNi_4]$ and $[RNi_5]$ subunits are dependent on the composition. Among them, R_2MgNi_9,[11,19] R_3MgNi_{14},[10,20] and R_4MgNi_{19} are the most interesting.[17,21]

In the La−Mg−Ni system, La_2MgNi_9 and La_3MgNi_{14} have already been studied as to their syntheses and crystal structures and hydrogen storage properties.[1–5,16–20] In contrast, the work on La_4MgNi_{19} was seldom reported until pure La_4MgNi_{19} can be prepared by sintering the powder mixture of $LaNi_{4.8}$ and Mg_2Ni at 900 °C for 10 days, followed by quenching to room temperature.[22,23] This preparation reveals that La_4MgNi_{19} has polymorphism with either a hexagonal (2H) or a rhombohedral (3R) structure.[23] However, the stability and formation condition of the 2H and 3R phases are unknown as well as the polymorphic transition between the two phases.

From a crystallographic point of view, the hexagonal and rhombohedral La_4MgNi_{19} phases crystallize in space groups $P6_3/mmc$ (no. 194) and $R\bar{3}m$ (no. 166), respectively.[17,23] Their unit cells consist of two and three blocks stacked along the *c* axis, respectively, constructing 2H and 3R structures. In both structures, each block is composed of one layer of $[LaMgNi_4]$ and three layers of $[LaNi_5]$, as illustrated in Figure 1. The structural distinction between the two variants exists only in the stacking mode of subunit layers. However, the differences in the equilibrium pressure for hydrogen absorption−desorption

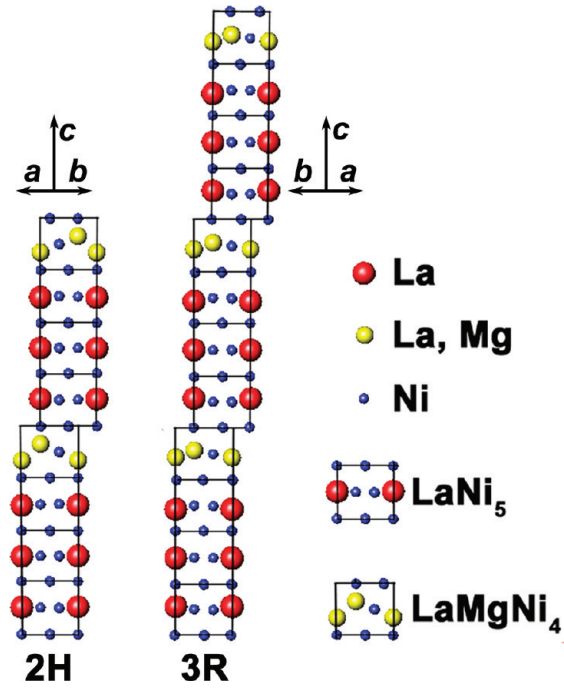

Figure 1. Structural stacking models for 2H- and 3R-type La_4MgNi_{19}. The La, (La+Mg), and Ni atoms are represented as red, yellow, and blue spheres, respectively.

* To whom correspondence should be addressed. E-mail: zhang03jp@yahoo.com.cn (Q.Z.), memzhu@scut.edu.cn (M.Z.).
† Anhui University of Technology.
‡ Fudan University.
§ South China University of Technology.

10.1021/jp103910e © 2010 American Chemical Society
Published on Web 06/11/2010

are undetectable by the normal measurement of the $P-C$ isotherm at 25 °C,[23,24] raising the question as to whether the two variants with different stacking modes have the same thermodynamics of hydrogen absorption and desorption. To clarify this question, it is necessary to measure their $P-C$ isotherms at different temperatures and further compare their X-ray diffraction (XRD) patterns under the same hydrogen pressure in the hydrogen absorption−desorption process. Moreover, the change in lattice strain with the hydriding−dehydriding process can be used to reveal the mechanism of hydrogen absorption−desorption.

In the present work, a systematic study of the La_4MgNi_{19} compound was carried out to determine the polymorphic transition and hydrogen absorption−desorption characteristics. First, the existence of the 2H and 3R variants was confirmed by crystallographic analyses. The polymorphic transition between the 2H and 3R phases was subsequently revealed by quenching the La_4MgNi_{19} samples at various temperatures, and a crystallographic model for this transition was proposed. The enthalpy changes for the hydrogen absorption and desorption of La_4MgNi_{19} were then determined from the $P-C$ isotherms measured at different temperatures. Finally, the XRD patterns for the 2H and 3R phases with hydrogen absorption and desorption were analyzed to explain the difference in performance and to reveal the change in lattice strain during the hydriding−dehydriding process.

Experimental Section

Sample Preparation. The La_4MgNi_{19} sample was prepared by the following steps: Appropriate amounts of pure metals were induction-melted under an argon atmosphere (about 0.1 MPa). About 3 wt % of La and 16 wt % of Mg were excessively added to compensate for the losses of La and Mg during melting. The as-obtained ingot was then mechanically crushed into 300-mesh powder and pressed into pellets that were wrapped in a tantalum foil and sintered at 900 °C for 48 h under an argon atmosphere (1 MPa) and then quenched to room temperature.

To investigate the influence of the sintering temperature on the polymorphic transition between the 2H and 3R phases, the quenched samples were again heated and kept at 840, 870, 930, and 960 °C for 10 h and then quenched to room temperature.

Structural Characterization. The microstructural and crystallographic characteristics of the La_4MgNi_{19} sample were investigated by electron backscatter diffraction (EBSD) in a field emission scanning electron microscope (FE-SEM), LEO SUPRA 55, with an energy-dispersive X-ray spectrometer (EDX). The bulk sample for the EBSD measurement was first mechanically and then electrochemically polished. Kikuchi patterns were generated at an acceleration voltage of 20 kV and recorded by a digital camera system. HKL-channel 5 software was used for EBSD acquisition and Kikuchi pattern analysis. Powder XRD measurements were carried out on a Rigaku D/Max 2500VL/PC diffractometer with Cu Kα radiation at 50 kV and 150 mA; the XRD patterns were refined by the Rietveld program RIETAN-2000.[25]

Hydrogen Absorption and Desorption. To investigate the hydrogen absorption and desorption properties of the La_4MgNi_{19} compound, the pressure−composition ($P-C$) isotherms were measured using a Sieverts-type apparatus at 25, 45, and 65 °C. Prior to formal measurements, the samples were fully activated by repeatedly hydriding−dehydriding at 100 °C four times. During each cycle, the samples were hydrided under a hydrogen pressure of 3 MPa for 1 h and subsequently dehydrided against a backpressure of 0.001 MPa for 1 h.

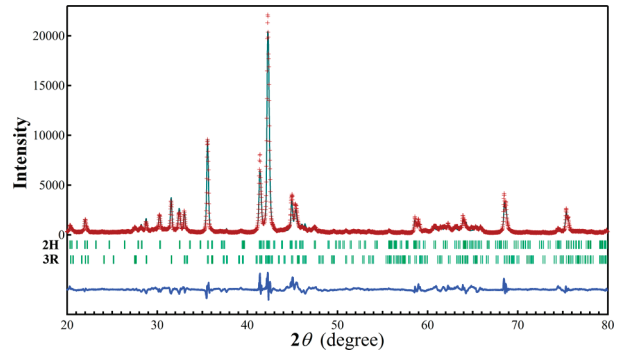

Figure 2. Rietveld refinement of the observed XRD pattern for the La_4MgNi_{19} sample quenched from 900 °C ($R_{wp} = 11.78\%$, $R_p = 9.14\%$, and $S = 2.87$).

To further understand the mechanism of hydrogen absorption−desorption for the 2H and 3R phases, the change in lattice strain during the hydrogen absorption−desorption process was investigated in detail. Because the equilibrium pressures of hydrogen absorption and desorption are fairly lower than 0.1 MPa at 25 °C,[23,24] it is appropriate to measure the XRD pattern of a hydrided La_4MgNi_{19} sample without decomposition under ambient conditions. Using the same method described previously,[26,27] a pseudo-Voigt function containing a Gaussian part and a Lorentzian part was chosen to fit the XRD peak profile in the Rietveld refinement. The lattice strains in the 2H and 3R phases caused by hydrogen absorption and desorption were extracted from the refined profile parameters.

Results and Discussion

Coexistence of 2H and 3R Phases. Figure 2 shows the Rietveld refinement of the XRD pattern of the La_4MgNi_{19} sample quenched from 900 °C with the coexistence of a hexagonal phase (2H) and a rhombohedral phase (3R), unlike a binary La_5Ni_{19} compound that exists only in a single 2H phase.[23] The appearance of a 3R phase suggests that the partial substitution of Mg for La in La_5Ni_{19} is favorable for the formation of the 3R phase and complies with the fact that the layered structure of an R−Ni compound is size-dependent,[28] that is, with the preference of a 2H structure for larger R atomic radii and the 3R structure for smaller R atomic radii. Thus, the coexistence of 2H and 3R phases in the La_4MgNi_{19} may be caused by the reduction in the average R atomic radius as the La (0.187 nm in radius) is partially substituted by the Mg (0.160 nm in radius).[29] The Rietveld analysis shows that the abundance of the 2H and 3R phases is 43 and 57 wt %, respectively.

The SEM/EDX analysis failed to determine the chemical compositions of the 2H and 3R phases in the La_4MgNi_{19} sample because these two phases cannot be distinguished from each other under SEM. Hence, EBSD was employed to reveal the microstructure. The EBSD map of the phase distribution in the La_4MgNi_{19} sample quenched from 900 °C is shown in Figure 3a, revealing clearly that there are two phases, colored in red and olive, respectively. The corresponding Kikuchi patterns (Figure 3b,c) for the red and olive regions can be well indexed to those patterns for the 2H and 3R phases with 46 wt % for the 2H phase and 54 wt % for the 3R phase. The phase amounts obtained here by the EBSD analysis agree well with the values revealed by the XRD Rietveld analysis. Figure 3d−f presents the EDX maps of La, Mg, and Ni, respectively, in the same area as the EBSD map (Figure 3a); La, Mg, and Ni elements are homogeneously dispersed in the 2H and 3R phases. The chemical compositions of the 2H and 3R phases are found to

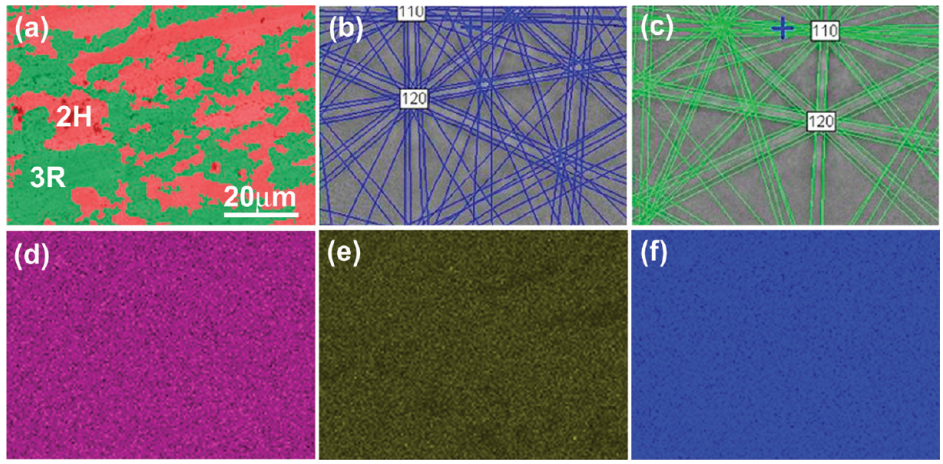

Figure 3. (a) EBSD map for 2H (red) and 3R (olive) phases in the sample quenched from 900 °C. (b, c) Kikuchi patterns of the 2H and 3R phases in (a), respectively. (d−f) EDX maps of La, Mg, and Ni, respectively.

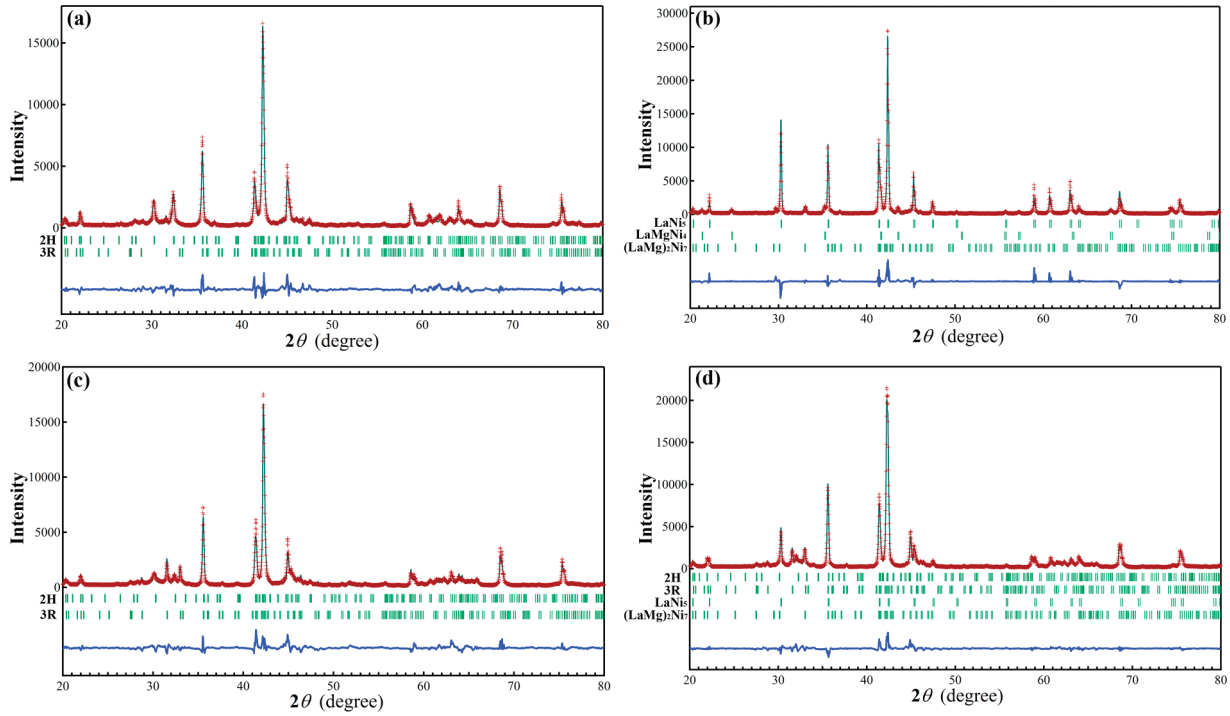

Figure 4. Rietveld refinements of observed XRD patterns for the La_4MgNi_{19} samples quenched from (a) 930 °C (R_{wp} = 12.28%, R_p = 9.37%, and S = 3.05), (b) 960 °C (R_{wp} = 11.92%, R_p = 9.54%, and S = 2.74), (c) 870 °C (R_{wp} = 12.19%, R_p = 9.52%, and S = 3.17), and (d) 840 °C (R_{wp} = 12.31%, R_p = 9.51%, and S = 2.85).

be nearly identical with the formulas of $La_{16.3\pm0.9}Mg_{3.9\pm0.6}Ni_{79.8\pm1.7}$ and $La_{16.1\pm1.1}Mg_{3.8\pm0.6}Ni_{80.1\pm1.5}$, respectively.

Because the composition is almost identical, the phase transition between the 2H and 3R phases does not need long-range atomic transport. As shown in Figure 1, each block in both structures includes one layer of [$LaMgNi_4$] and three layers of [$LaNi_5$], although two blocks stacked along the c axis form one period of 2H structure while three blocks construct a unit cell of the 3R structure. It is thus possible that the transition between the two phases may be realized by a slight displacement of subunit layers, which will be further discussed below.

Stability and Transition between 2H and 3R. To reveal the temperature dependence of the transition between the 2H and 3R phases, the sample quenched from 900 °C was reheated and kept at 840, 870, 930, and 960 °C for 10 h and then requenched to room temperature. The XRD pattern for the La_4MgNi_{19} sample quenched from 930 °C is presented in Figure 4a and shows that the sample still consists of 2H and 3R phases.

When the quenching temperature is increased to 960 °C, 2H and 3R phases are absent but replaced by three new phases: $LaNi_5$, $LaMgNi_4$, and $(La,Mg)_2Ni_7$ (see Figure 4b). Referring to the La−Ni phase diagram,[13,17] one may deduce that, at 960 °C, La_4MgNi_{19} decomposes into $LaNi_5$ and a liquid phase via a peritectic reaction, namely

$$La_4MgNi_{19} \rightarrow LaNi_5 + \text{liquid phase} \qquad (1)$$

where the liquid phase would be resolidified into $LaMgNi_4$ and $(La,Mg)_2Ni_7$ in the subsequent quenching process. Figure 5 shows the backscattered SEM image of the La_4MgNi_{19} sample quenched from 960 °C, where the resolidified phases along the grain boundaries of the $LaNi_5$ are clearly visible.

Conversely, as the quenching temperature is decreased to 870 °C, 2H and 3R phases remain (see Figure 4c), but two more phases ($LaNi_5$ and $(La,Mg)_2Ni_7$) appear as the temperature is

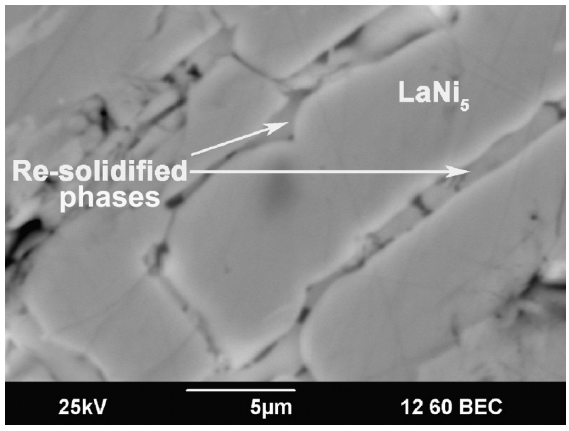

Figure 5. Backscattered SEM image of the La_4MgNi_{19} sample quenched from 960 °C.

TABLE 1: Lattice Parameters and Abundance of Each Phase in Quenched La_4MgNi_{19} Samples

quenching temp (°C)	phases	lattice parameters (Å)		abundance (wt %)
		a	*c*	
960	$LaNi_5$	5.0319(2)	3.995(4)	79
	$(La,Mg)_2Ni_7$	5.0389(1)	24.227(5)	16
	$LaMgNi_4$	7.1894(9)		5
930	2H-type La_4MgNi_{19}	5.0333(3)	32.327(1)	84
	3R-type La_4MgNi_{19}	5.0330(5)	48.248(1)	16
900	2H-type La_4MgNi_{19}	5.0319(2)	32.278(4)	43
	3R-type La_4MgNi_{19}	5.0325(6)	48.223(2)	57
870	2H-type La_4MgNi_{19}	5.0298(4)	32.261(7)	32
	3R-type La_4MgNi_{19}	5.0323(3)	48.211(1)	68
840	2H-type La_4MgNi_{19}	5.0284(3)	32.243(6)	21
	3R-type La_4MgNi_{19}	5.0318(7)	48.193(3)	40
	$LaNi_5$	5.0294(1)	3.994(3)	20
	$(La,Mg)_2Ni_7$	5.0365(2)	24.197(7)	19

further decreased to 840 °C (see Figure 4d), meaning that some of the La_4MgNi_{19} decomposed into $LaNi_5$ and $(La,Mg)_2Ni_7$ at 840 °C, namely

$$La_4MgNi_{19} \rightarrow LaNi_5 + (La,Mg)_2Ni_7 \quad (2)$$

From the results above, it is evident that a pure La_4MgNi_{19} compound exists in the temperature range of 840−960 °C, which is below the range of 900−1000 °C for the binary La_5Ni_{19} compound.[13]

The abundance of each phase in the quenched La_4MgNi_{19} samples was obtained by Rietveld refinements on XRD data (see Table 1). The relative amount of the 2H phase decreases from 84 to 32 wt % as the quenching temperature is lowered from 930 to 870 °C, indicating that the 2H phase is thermodynamically stable at a higher temperature and will be transformed into the 3R phase if the temperature decreases. Unfortunately, the exact transition temperature between the two phases was not determined due to the failure of obtaining a single-phase sample in the experiments, as was also the case of binary R_2Ni_7 compounds.[28] A possible reason is that the driving force for this transition is too small because the two phases are slightly different in both structure and composition, which is why their mutual transition is less affected by changing the heating temperature.[28]

As an example, the transition from the 2H phase to the 3R phase in the La_4MgNi_{19} compound is proposed in Figure 6, which meets the requirement that the chemical compositions of the two phases are identical without requiring the long-range atomic transport. The stacking blocks of the 2H and 3R structures can be seen as the AB- and ABC-type, respectively. Block A upon the 2H unit cell can be converted into block C of the 3R structure with a slip by $2a/3 + b/3$ (i.e., $^1/_3$ in the [210] direction), which is equivalent to the slip by $-a/3 + b/3$ or $-a/3 - 2b/3$. On the contrary, block B beneath the 2H unit cell is slipped by $-2a/3 - b/3$ to form block C of the 3R structure. Meanwhile, the $[LaMgNi_4]$ subunit at the connection between the slip and nonslip blocks (see Figure 6) has to be adjusted for accommodation; that is, the (La+Mg) layer at the slip side shifts together with the slip block, and the nonslip side remains without slip while the Ni layer between the two (La+Mg) layers shifts in the reverse direction. The polymorphic transition from the 3R phase to the 2H phase may follow the reverse process.

Hydrogen Absorption and Desorption by La_4MgNi_{19}. Figure 7a shows the $P-C$ isotherms at 25, 45, and 65 °C for the La_4MgNi_{19} sample quenched from 900 °C. Obviously, only one flat plateau can be seen on each curve at each temperature, suggesting that 2H and 3R phases have quite close equilibrium pressures upon hydrogen absorption and desorption, which does not mean that they are exactly the same because of the limited precision of the pressure transducer.

By taking the equilibrium pressures from the $P-C$ isotherms in Figure 7a, the van't Hoff plots for the $La_4MgNi_{19}-H_2$ system were obtained and are displayed in Figure 7b. Because the equilibrium pressures for the 2H and 3R phases are very close to each other, the enthalpy changes are averaged and determined to be −32.1 kJ/mol H_2 for absorption and 31.5 kJ/mol H_2 for desorption. These values are close to the ±30 kJ/mol H_2 for the $LaNi_5-H_2$ system.[30]

The comparison of the present values with the reported data for other layered compounds, such as RNi_3 and R_2Ni_7, indicates that the hydride formation enthalpies for the ternary compounds, which are near −30 kJ/mol H_2 (for example, −31.4 kJ/mol H_2 for $La_{1.5}Mg_{0.5}Ni_7$), are numerically smaller than the enthalpies around −44 kJ/mol H_2 for the binary compounds, such as $CeNi_3$ and Ce_2Ni_7.[31,32] This change in thermodynamics due to partial replacement of La by Mg may be related to the fact that both $[RMgNi_4]$ and $[RNi_5]$ subunits in the ternary compounds are randomly occupied by hydrogen, whereas only $[R_2Ni_4]$ subunits in the binary compounds are occupied exclusively.[21,24,31,33]

Mechanism of Hydrogen Absorption and Desorption. To investigate the structural change of the 2H and 3R phases during hydrogen absorption and desorption processes, the La_4MgNi_{19} sample quenched from 900 °C was selected due to the easy comparison between the 2H and 3R phases, and the measured XRD patterns are presented in Figure 8, from which the following three features can be extracted:

(i) Hydrogen absorption is accompanied with the phase transformation from a H-dissolved solid solution to a full hydride, and hydrogen desorption follows the reverse process. At the initial stage of absorption, the lattice expansion caused by the dissolved hydrogen in the host lattice leads to the shifting of XRD peaks toward a lower angle with an increase in the hydrogen content to 0.13 wt % (see Figure 8a). As the hydrogen content increases to 0.31 wt % and brings about the formation of a hydride, the coexistence of an H-dissolved solid solution and a hydride is thus observed. With further hydrogen absorption at the final stage (the hydrogen pressure increases to 0.075 MPa), more hydrogen atoms enter the hydride lattice so that the XRD peaks of the hydride are further shifted toward a much lower angle. Nevertheless, in the whole hydriding process, no intermediate hydride is observed, in contrast to the phenomenon

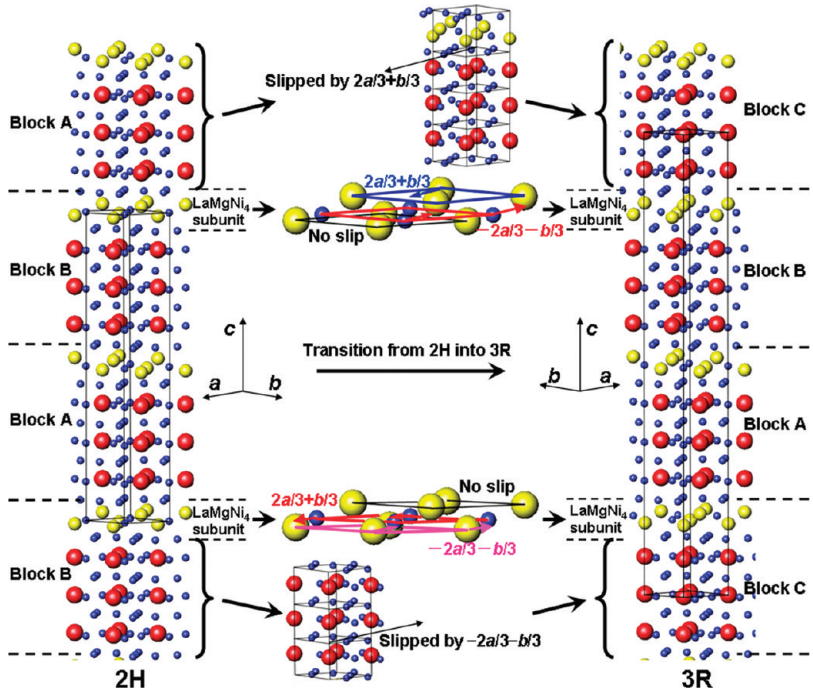

Figure 6. Schematic illustration of the polymorphic transition from 2H into 3R in a La_4MgNi_{19} compound. The La, (La+Mg), and Ni atoms are represented as red, yellow, and blue spheres, respectively.

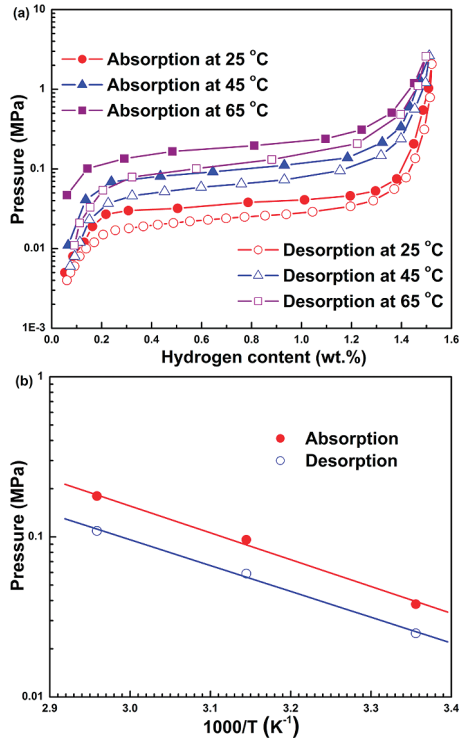

Figure 7. (a) $P-C$ isotherms of hydrogen absorption and desorption for the La_4MgNi_{19} sample quenched from 900 °C. (b) The van't Hoff plots for a $La_4MgNi_{19}-H_2$ system.

occurring in the cubic $LaMgNi_4$ compound where the orthorhombic $LaMgNi_4H_{3.7}$ is produced prior to the formation of the cubic $LaMgNi_4H_{4.85}$.[34] Such a feature complies with the typical characteristics of interstitial hydrides represented by the $LaNi_5-H_2$ system.[35,36]

(ii) The (110) peak for the 3R phase is always positioned at the right-hand side of the (110) peak for the 2H phase in either hydrogen absorption or hydrogen desorption. These two (110) peaks overlap with each other only when the sample is in a fully hydrided or dehydrided state (see Figure 8). Thus, it is reasonable to deduce that the 3R phase absorbs hydrogen behind the 2H phase, but the 3R hydride desorbs hydrogen ahead of the 2H hydride. This deduction is supported by the change in the cell volume of the 2H phase and 3R phase during hydrogen absorption and desorption (Table SI-1, Supporting Information), suggesting further that the equilibrium pressures of hydrogen absorption and desorption for the 2H phase should be lower than the pressures for the 3R phase, albeit the difference is too small to be distinguished from the $P-C$ isotherms (see Figure 7a). This result can be explained by the lattice parameters of the 2H and 3R phases that were obtained by the Rietveld refinement on XRD data. As shown in Table 1, the a-axis lengths of subunits in the 2H and 3R phases for the sample quenched from 900 °C are close to each other (5.0319 versus 5.0325 Å, respectively), but the average c-axis length of subunits in the 2H phase (4.0348 Å) is slightly larger than the length (4.0186 Å) in the 3R phase. Hence, it is likely that the equilibrium pressures of hydrogen absorption and desorption are dependent on the subunit sizes of these layered structures.

(iii) Peak broadening, as observed in the 2H and 3R H-dissolved solid solution phases, significantly increases with the increase of hydrogen content; however, the Bragg peaks abruptly sharpen once the hydrides are formed from the corresponding H-dissolved solid solution phases and become much sharper as the hydrogen content increases further (see Figure 8a). Note that the subsequent desorption measurements show the reverse process (see Figure 8b), confirming that the peak broadening is due to the increase in lattice strain rather than the reduction in crystallite size. Figure 9 shows the lattice strains for the 2H and 3R phases during hydrogen absorption and desorption. Both the H-dissolved solid solution phase and the hydride show their maximum lattice strains in the two-phase region, but the latter strain is apparently less than the former strain. This feature is identical for both the 2H and the 3R structures, implying that the 2H and 3R phases have the same mechanism of hydrogen absorption and desorption. Previous

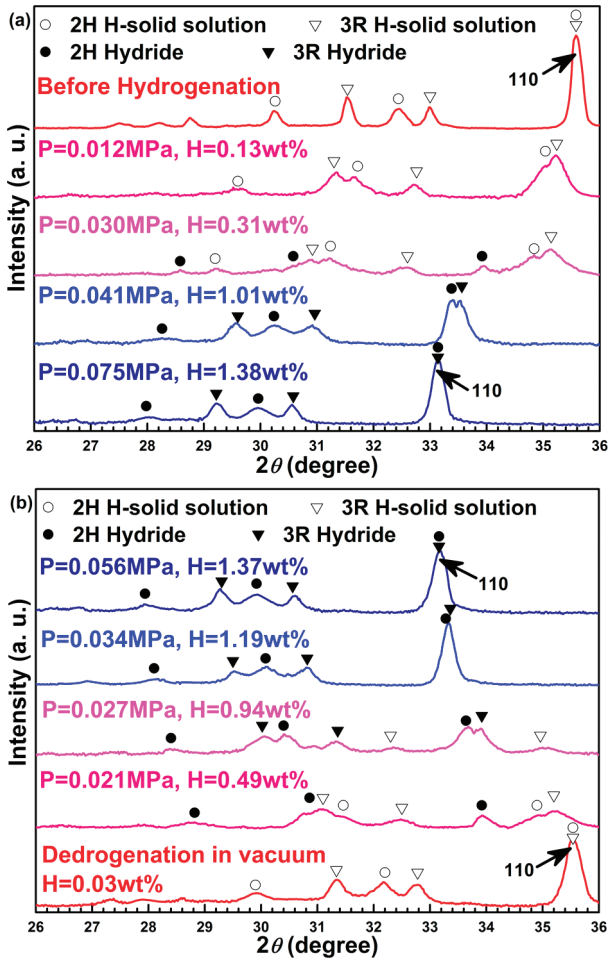

Figure 8. XRD patterns of a La_4MgNi_{19} sample quenched from 900 °C after hydrogen (a) absorption and (b) desorption. The hydrogen contents in the hydrided and dehydrided samples were measured using a LECO RH-404 hydrogen determinator.

studies by neutron diffraction confirm that hydrogen more preferentially occupies the interstitial sites of the Laves-type subunits than those of the AB_5-type subunits in a layered compound.[31,37,38] Hence, it is reasonable to assume that mainly hydrogen atoms fill the [$LaMgNi_4$] subunits in the 2H and 3R H-dissolved solid solution phases. The H-induced expansion of the basal plane of the [$LaMgNi_4$] subunits is constrained by the connected [$LaNi_5$] subunits, which gives rise to a significant lattice strain.[24,31,33,38] The lattice strain would be released once hydrogen atoms begin to occupy the [$LaNi_5$] subunits to form a hydride. Hence, the lattice strains in both the full 2H and 3R hydrides are less than their corresponding H-dissolved solid solution phases.

In short, the 2H and 3R phases show almost the same behavior with regard to hydrogen absorption and desorption, except that the 2H phase has slightly lower equilibrium pressures than the 3R phase. The changes in the lattice strain for 2H and 3R phases suggest that the hydrogen atoms fill the interstices in [$LaMgNi_4$] subunits first; then the interstices in [$LaNi_5$] subunits are filled next in hydrogen absorption. The reverse process may occur in hydrogen desorption; that is, the hydrogen atoms empty from the interstices in [$LaNi_5$] subunits first and then from the interstices in [$LaMgNi_4$] subunits. This sequence should be further verified by means of dynamic in situ neutron diffraction.

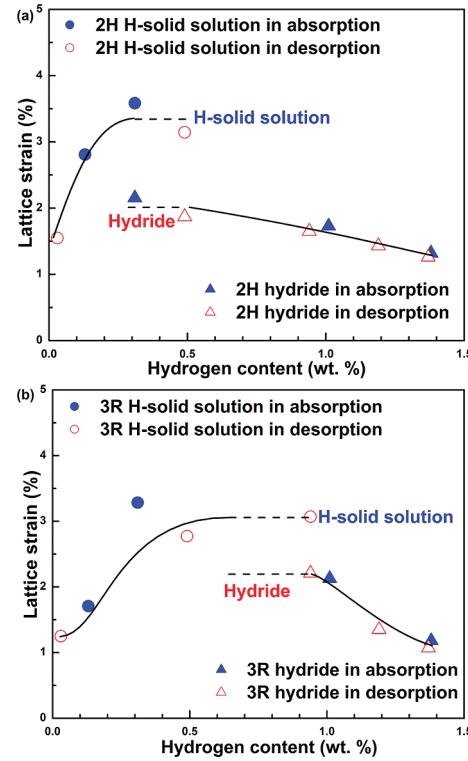

Figure 9. Lattice strains in (a) 2H and (b) 3R phases during hydrogen absorption and desorption. Note that the abscissa represents the hydrogen content for mixed 2H and 3R phases, not the hydrogen content in single 2H or 3R phases.

Conclusions

A systematic investigation of the phase stability, structural transition, and hydrogen absorption−desorption characteristics of the polymorphic La_4MgNi_{19} compound was conducted. The present work shows that a La_4MgNi_{19} compound existing in a temperature range of 840−960 °C has two variants, viz., a hexagonal structure (2H) stabilizing at a higher temperature and a rhombohedral structure (3R) stabilizing at a lower temperature. The polymorphic transition between 2H and 3R structures does not need long-range atomic transport due to identical composition. The equilibrium pressures of hydrogen absorption and desorption for the 2H phase are lower than the pressures for the 3R phase, but they are barely distinguishable from the measured $P-C$ isotherms. The average hydriding and dehyriding enthalpies are determined to be −32.1 and 31.5 kJ/mol H_2, respectively. The lattice strains in both the 2H and the 3R structures progressively increase with an increase in the hydrogen content in H-dissolved solid solution phases but dramatically decrease once the H-dissolved solid solution phases transform fully into the corresponding hydrides, suggesting that hydrogen atoms first fill the interstitial sites in [$LaMgNi_4$] subunits for 2H and 3R H-dissolved solid solution phases and then fill the interstitial sites in [$LaNi_5$] subunits for hydride phases.

Acknowledgment. This work was financially supported by the National Natural Science Foundation of China (Nos. 50771001, 50971001, and 50925102) and the National Basic Research Program of China (No. 2010CB631302).

Supporting Information Available: The change in the cell volume (Table SI-1) of 2H phase and 3R phase during hydrogen absorption and desorption (at 25 °C). This material is available free of charge via the Internet at http://pubs.acs.org.

References and Notes

(1) Kadir, K.; Sakai, T.; Uehara, I. *J. Alloys Compd.* **1997**, *257*, 115–121.
(2) Pan, H. G.; Liu, Y. F.; Gao, M. X.; Li, R.; Lei, Y. Q. *Intermetallics* **2005**, *13*, 770–775.
(3) Ozaki, T.; Kanemoto, M.; Kakeya, T.; Kitano, Y.; Kuzuhara, M.; Watada, M.; Tanase, S.; Sakai, T. *J. Alloys Compd.* **2007**, *446/447*, 620–624.
(4) Chai, Y. J.; Sakaki, K.; Asano, K.; Enoki, H.; Akiba, E.; Kohno, T. *Scr. Mater.* **2007**, *57*, 545–548.
(5) Kadir, K.; Kuriyama, N.; Sakai, T.; Uehara, I.; Eriksson, L. *J. Alloys Compd.* **1999**, *284*, 145–154.
(6) Liang, G.; Schulz, R. *J. Alloys Compd.* **2003**, *356/357*, 612–616.
(7) Miraglia, S.; Girard, G.; Fruchart, D.; Liang, G.; Huot, J.; Schulz, R. *J. Alloys Compd.* **2009**, *478*, L33–L36.
(8) Escobar, D.; Srinivasan, S.; Goswami, Y.; Stefanakos, E. *J. Alloys Compd.* **2008**, *458*, 223–230.
(9) Tanaka, H.; Senoh, H.; Kuriyama, M.; Aihara, K.; Terashita, N.; Nakahata, T. *Mater. Sci. Eng., B* **2004**, *108*, 81–90.
(10) Si, T. Z.; Pang, G.; Zhang, Q. A.; Liu, D. M.; Liu, N. *Int. J. Hydrogen Energy* **2009**, *34*, 4833–4837.
(11) Si, T. Z.; Zhang, Q. A.; Pang, G.; Liu, D. M.; Liu, N. *Int. J. Hydrogen Energy* **2009**, *34*, 1483–1488.
(12) Zhang, J.; Fang, F.; Zheng, S.; Zhu, J.; Chen, G.; Sun, D.; Latroche, M.; Percheron-Guégan, A. *J. Power Sources* **2007**, *172*, 446–450.
(13) Yamamoto, T.; Inui, H.; Yamaguchi, M.; Sato, K.; Fujitani, S.; Yonezu, I.; Nishio, K. *Acta Mater.* **1997**, *45*, 5213–5221.
(14) Zhang, J.; Zhou, G.; Chen, G.; Latroche, M.; Percheron-Guégan, A.; Sun, D. *Acta Mater.* **2008**, *56*, 5388–5394.
(15) Zhang, Q. A.; Pang, G.; Si, T. Z.; Liu, D. M. *Acta Mater.* **2009**, *57*, 2002–2009.
(16) Kohno, T.; Yoshida, H.; Kawashima, F.; Inaba, T.; Sakai, I.; Yamamoto, M.; Kanda, M. *J. Alloys Compd.* **2000**, *311*, L5–L7.
(17) Hayakawa, H.; Akiba, E.; Gotoh, M.; Kohno, T. *Mater. Trans.* **2005**, *46*, 1393–1401.
(18) Khan, Y. *Acta Crystallogr.* **1974**, *B30*, 1533–1537.
(19) Shi, S.; Li, C.; Tang, W. *J. Alloys Compd.* **2009**, *476*, 874–877.
(20) Chai, Y.; Asano, K.; Sakaki, K.; Enoki, H.; Akiba, E. *J. Alloys Compd.* **2009**, *485*, 174–180.
(21) Nakamura, Y.; Nakamura, J.; Iwase, K.; Akiba, E. *Nucl. Instrum. Methods Phys. Res., Sect. A* **2009**, *600*, 297–300.
(22) Hayakawa, H.; Enoki, H.; Akiba, E. *J. Jpn. Inst. Met.* **2006**, *70*, 158–161.
(23) Ferey, A.; Cuevas, F.; Latroche, M.; Knosp, B.; Bernard, P. *Electrochim. Acta* **2009**, *54*, 1710–1714.
(24) Nakamura, J.; Iwase, K.; Hayakawa, H.; Nakamura, Y.; Akiba, E. *J. Phys. Chem. C* **2009**, *113*, 5853–5859.
(25) Izumi, F.; Ikeda, T. *Mater. Sci. Forum* **2000**, *321/323*, 198–203.
(26) Larson, A. C.; Von Dreele, R. B. *GSAS-General Structure Analysis System*; Los Alamos National Laboratory Report No. LAUR 86-748; Los Alamos National Laboratory: Los Alamos, NM, 1994; p 127.
(27) Nakamura, Y.; Bowman, R. C.; Akiba, E. *J. Alloys Compd.* **2004**, *373*, 183–193.
(28) Buschow, K. H. J.; van Der Goot, A. S. *J. Less-Common Met.* **1970**, *22*, 419–428.
(29) Wilson, A. J. C. *International Tables for Crystallography C*; Kluwer Academic Publishers: Boston, MA, 1992; p 681.
(30) van Vucht, J. H. N.; Kuijpers, F. A.; Bruning, H. C. A. M. *Philips. Res. Rep.* **1970**, *25*, 133–140.
(31) Denys, R. V.; Riabov, A. B.; Yartys, V. A.; Sato, M.; Delaplane, R. G. *J. Solid State Chem.* **2008**, *181*, 812–821.
(32) Denys, R. V.; Yartys, V. A.; Sato, M.; Riabov, A. B.; Delaplane, R. G. *J. Solid State Chem.* **2007**, *180*, 2566–2576.
(33) Filinchuk, Y. E.; Yvon, K.; Emerich, H. *Inorg. Chem.* **2007**, *46*, 2914–2920.
(34) Chotard, J. N.; Sheptyakov, D.; Yvon, K. *Z. Kristallogr.* **2008**, *223*, 690–696.
(35) Nakamura, Y.; Bowman, R. C.; Akiba, E. *J. Alloys Compd.* **2007**, *431*, 148–154.
(36) Nakamura, Y.; Akiba, E. *J. Alloys Compd.* **2000**, *308*, 309–318.
(37) Filinchuk, Y. E.; Sheptyakov, D.; Yvon, K. *J. Alloys Compd.* **2006**, *413*, 106–113.
(38) Yartys, V. A.; Isnard, O.; Riabov, A. B.; Akseirud, L. G. *J. Alloys Compd.* **2003**, *356/357*, 109–113.

JP103910E